

Cross-linking controls the mechanical properties of protein crystals

Daiki Takaku ¹, Ryo Suzuki ^{1,2}, Kenichi Kojima,¹ and Masaru Tachibana ^{1,*}¹Graduate School of Nanobioscience, Yokohama City University, 22-2 Seto, Kanazawa-ku, Yokohama 236-0027, Japan²Precursory Research for Embryonic Science and Technology (PRESTO), Japan Science and Technology Agency (JST), 4-1-8 Honcho, Kawaguchi, Saitama 332-0012, Japan

(Received 10 January 2024; accepted 29 April 2024; published 30 May 2024)

Mechanical properties such as plasticity are fundamental and important properties in processing and applications of materials. Protein crystals are one of the macroscopic molecular crystals composed of protein molecules with nanometer size. The application of protein crystals has been explored not only for the structure analysis of proteins, but also for their application as solids. Generally, it is known that native protein crystals are quite brittle. However, it is empirically known that the mechanical property of protein crystals is enhanced by a cross-linking technique. One of the qualitative reasons is that chemical cross-linking enhances the mechanical strength, but the detailed mechanical properties are not clear. Herein, we investigate the macroscopic elastic and plastic behaviors of cross-linked tetragonal hen-egg-white lysozyme crystals under a compression test. The cross-linked crystals exhibit plastic deformation whereas the native crystals show brittle fracture. The plastic behavior of the cross-linked crystals clearly shows yield phenomena with upper and lower yield points. Stress-induced dislocations are also noted. The Burgers vectors of the moving dislocations of the crystals are characterized by synchrotron x-ray topography, and the results indicate that the slip systems are controlled by cross-linking. Thus, cross-linking leads to the macroscopic plastic deformation of protein crystals. The ductile properties of the cross-linked protein crystals indicate their great potential for material applications such as biocatalysis and biosensing.

DOI: [10.1103/PhysRevMaterials.8.L052601](https://doi.org/10.1103/PhysRevMaterials.8.L052601)

Introduction. Plasticity and ductility are fundamental and important properties in the processing and applications of various materials. The plastic deformation of crystalline materials is caused by dislocation, multiplication, and motion, which have been widely investigated for many metals and semiconductor crystals [1]. Studying the dislocation behaviors of crystalline materials is important to understand their mechanical properties.

Protein crystals are solid materials composed of biomacromolecules. Obtaining single protein crystals is crucial for understanding the structure of protein molecules. The molecular size of protein crystals is on the order of nanometers; thus, a large intermolecular distance and pore size of over 10 nm distinguish these materials from common inorganic and low-molecular-weight organic crystals. In addition, protein crystals contain large amounts of intracrystalline water (~70 vol%) [2,3]. Thus, the presence of porosity within protein crystals enables the introduction of additives to bring out new material properties. The application of such porous structures holds promise for the development of new biomaterials. Therefore, the application of protein crystals has been explored not only for the structure analysis of proteins, but also for their application as biomaterials [4].

The mechanical properties of protein crystals, such as their elasticity and plasticity, have been evaluated so far. Native protein crystals are generally fragile [5] and their hardness

is sensitive to environmental conditions such as humidity [6] because these crystals are crystallized by weak interactions, such as van der Waals forces, electrostatic forces, and the hydrogen bonds associated with intracrystalline water. Recently, it was reported that crystallization with additives such as gel media is useful to improve the fragility of these crystals [7]. The fracture stress of a crystal grown with 1.0 wt% gel (2.12 MPa) is approximately ten times larger than that of native crystals (0.29 Mpa) [7]. Additives can also drastically improve the fracture stress of these crystals.

The cross-linking method has attracted much attention for enhancing the strength of protein crystals. Cross-linked protein crystals are empirically strong and can be handled directly by mechanical contact without breakage [8]. Moreover, they are usually stable and insoluble in water and organic solutions [9]. In the case of crystals composed of atoms, such as metals and inorganic materials, the precise modulation of intersite bonding forces within the established crystal lattice structure presents a significant challenge. In contrast, protein crystals exhibit a unique capacity to exert control over these bonding forces through the strategic introduction of covalent bonds facilitated by cross-linking between lattice sites. This feature can be regarded as a significant characteristic of protein crystals with inherent porosity. Cross-linking forms covalent bonds between the amino acid residues of protein molecules [10]. Glutaraldehyde is a commonly used cross-linker because of its ease of handling and high efficacy.

In pioneering research, the mechanical properties, such as the Young's modulus, of cross-linked triclinic hen-egg-white

*tachiban@yokohama-cu.ac.jp

lysozyme (HEWL) crystals was estimated to be 210 MPa by using transverse resonance vibrations in the frequency range 1–100 kHz [11]. Dynamic Young's moduli of 3.21 and 0.58–3.20 GPa in ultrahigh-frequency (mega- and gigahertz) regions have been measured in tetragonal HEWL (T-HEWL) crystals by using ultrasonic pulse echo and the Brillouin scattering method, respectively [12–14]. The microscopic mechanical properties of cross-linked T-HEWL crystals have been investigated using the nanoindentation method [9,15]. The macroscopic mechanical properties of cross-linked protein crystals must be characterized to obtain a comprehensive understanding of these crystals and expand their applications. However, to the best of our knowledge, no reports on such characterizations have yet been published.

Herein, we investigated the macroscopic elastic and plastic behaviors of cross-linked T-HEWL crystals using an Instron autograph instrument. The results revealed that the cross-linked protein crystals had noticeably improved mechanical properties, which transitioned from brittle to ductile characteristics owing to cross-linking among the protein molecules. To the best of our knowledge, this phenomenon has not been observed in any other material, although the brittle-ductile transition owing to temperature changes has been observed. In addition, the plastic behavior of the crystals exhibited yield phenomena with upper and lower yield points. The appearance of a slip line suggests that plastic deformation is controlled by a dislocation mechanism. The slip plane and Burgers vector of the slip dislocation were determined using synchrotron x-ray topography. Macroscopic plastic deformation occurred even in brittle protein crystals because of cross-linking.

Experimental methods: Preparation of the specimens. Once-crystallized HEWL was purchased from Nacalai Tesque, Inc., and used without further purification. T-HEWL crystals ($P4_32_12$, $a = b = 79.1 \text{ \AA}$, $c = 37.9 \text{ \AA}$, $Z = 8$) were grown via a salt-concentration gradient method at 296 K in test tubes held vertically using NiCl_2 as a precipitant [16]. Almost all crystals exhibited similar growth planes, such as the $\{110\}$ and $\{101\}$ planes. The crystal size was approximately 2–4 mm.

Chemical cross-linking was performed by soaking. Glutaraldehyde was purchased from Wako Pure Chemical Industries, Ltd., and used without further purification. The chemical cross-linking solution was prepared by adding 2.5 wt% glutaraldehyde to a solution containing the same precipitant (11.6 wt% NiCl_2) as the original solution used for crystallization. The cross-linked crystals were obtained by controlling the cross-linking time. Native crystals were immersed in this solution at 296 K for 1–7 days. The lattice parameters of cross-linked HEWL crystals are slightly shorter than those of native ones [17]. For comparison, the lattice parameters of both types of crystals are summarized in Table I. The crystal size was measured using an optical microscope. The contact areas and heights of the specimens were measured using optical micrographs and ImageJ software [18].

Experimental methods: Compression test. Compression tests were performed on an Instron autograph machine (Shimadzu, AGS-X) at $296 \pm 2 \text{ K}$. The crystals were covered with the precipitant solution to prevent water evaporation and placed on the stage of the instrument. The crystals were

TABLE I. Lattice parameters of native and cross-linked T-HEWL crystals.

Lattice parameter (nm)	Native (PDB: 1lyz [17])	Cross-linked ^a (PDB: 2hu3 [10])
a	7.91	7.89
b	7.91	7.89
c	3.79	3.70

^aNote that the cross-linking time was 24 h [10].

compressed using two parallel stainless-steel plates, one with a load cell attached and the other with a sample stage, at a compression rate of 50 $\mu\text{m}/\text{min}$. The strain rate was $4 \pm 2 \times 10^{-4} \text{ s}^{-1}$ because the compression tests were conducted on grown crystals with heights of 1.5 to 3.5 mm. During the measurements, the compressive plane and axis corresponded to the (110) and $[\bar{1}\bar{1}0]$ planes, respectively.

Experimental methods: Characterization of dislocations by x-ray topography. Synchrotron x-ray topography with a monochromatic beam was performed at 296 K on the BL20B beamline at the Photon Factory of the High-Energy Accelerator Research Organization (KEK). A monochromatic beam of 1.2 \AA was selected by adjusting the double-crystal monochromator. The crystals were gently transferred into a transparent polypropylene straw. The evaporation of the water contained in the crystal was avoided by covering it with the precipitant solution, and both sides of the straw were sealed with Parafilm. The sealed straw was mounted on a precision goniometer and rotated in high-resolution angular steps around the Bragg diffraction angle. A series of diffraction images were collected using a high-spatial-resolution two-dimensional (2D) digital x-ray charge-coupled device (CCD) camera (Photonic Science X-RAY FDI 1.00:1, effective pixel size $6.45 \times 6.45 \mu\text{m}^2$) with a total exposure time of several minutes. The CCD camera outputs sequential x-ray topographs as 16-bit greyscale TIFFs. These images are easily analyzed using free software such as ImageJ [18]. ImageJ software can draw three stack-type images as Z projections. The dislocation images were reconstructed using the median value of the diffraction intensity, as reported previously [19]. X-ray topographs with a spatial resolution of 2 μm were obtained using x-ray films (Structurix D2, AGFA) with an exposure time of 180 s. X-ray topography is a powerful tool for identifying crystal defects such as dislocations.

Results and discussion: Stress-strain curves of native and cross-linked protein crystals. Figures 1(a) and 1(b) show the stress-strain curves of native and one-week-cross-linked T-HEWL crystals obtained under compression. Here, stress and strain refer to the nominal stress and strain, respectively. Stress and strain showed a linear relationship in the curves of both the native and one-week-cross-linked crystals. This linear region corresponds to elastic deformation. Red lines in Figs. 1(a) and 1(b) were extrapolated from the slope of the elastic region.

We assessed the elastic and plastic regions of the stress-strain curves. The static Young's modulus of the crystals was estimated from the slope of the linear region of their stress-strain curves. The Young's moduli of the native and

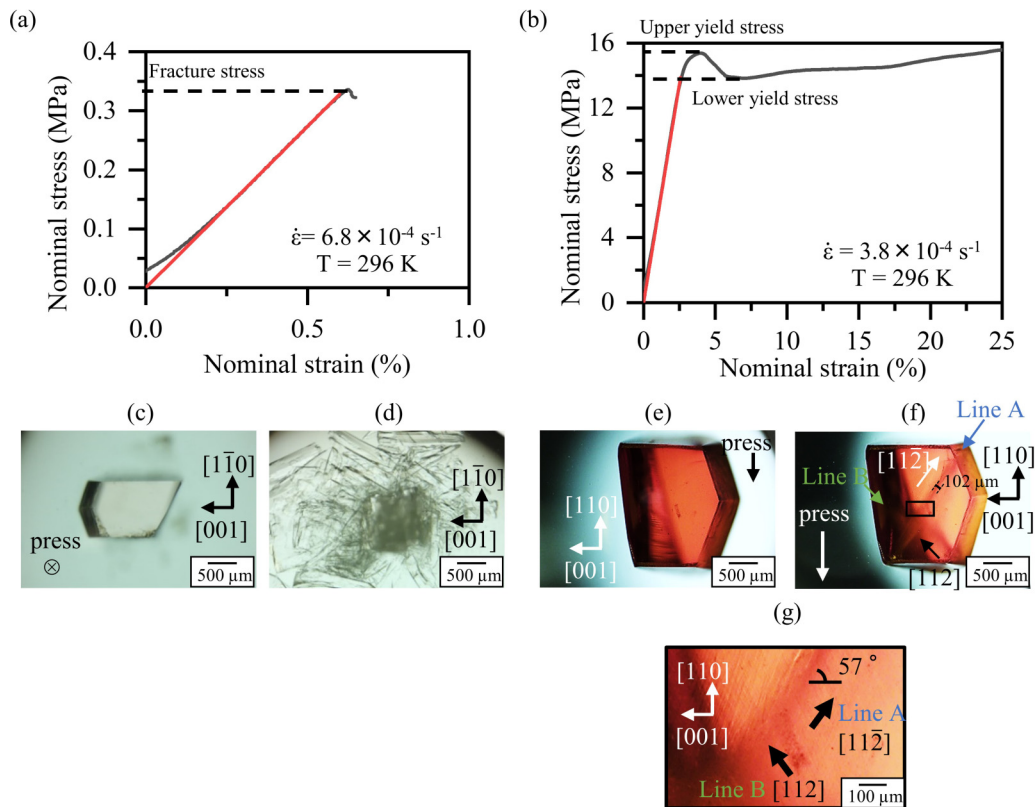


FIG. 1. Typical stress-strain curves of (a) native and (b) 1-week-cross-linked protein crystals at 296 K. The strain rate is $\sim 10^{-4} \text{ s}^{-1}$. Red lines are extrapolated as the slope of the elastic region. $\dot{\epsilon}$ and T in the figure indicate the strain rate and temperature during the compression test, respectively. Optical micrographs of the [(c), (d)] native and [(e), (f)] 1-week cross-linked crystals [(c), (e)] before and [(d), (f)] after the compression test. (g) Magnification of the area marked by the rectangle in (f). Slip traces in the $[112]$ and $[11\bar{2}]$ directions are denoted by arrows.

one-week-cross-linked crystals were 67.5 ± 22.6 and 379 ± 80.6 MPa, respectively. The static Young's modulus of the native crystals was comparable with that of previously reported native and gel-incorporated crystals (63 MPa) [7]. By contrast, the static Young's modulus of the one-week-cross-linked crystals increased drastically compared with that of the native crystals owing to the strong intermolecular forces induced by cross-linking with glutaraldehyde. The Young's modulus of the one-week-cross-linked crystals was comparable with that of a previously reported cross-linked crystal (210 MPa) [11] but lower than that of cross-linked crystals measured using the nanoindentation method (1080 MPa) [15]. This discrepancy may be related to the test scale between macroscopic and microscopic deformations.

When the maximum stress was achieved in the elastic region of the stress-strain curve of the native crystals, the stress abruptly decreased with increasing strain, and fracture occurred simultaneously. Optical micrographs of the native crystals before and after compression are shown in Figs. 1(c) and 1(d), respectively. Numerous cracks and fragments could be observed in the compressed crystals. This behavior corresponds to typical brittle fractures. The maximum stress in the stress-strain curve of the native crystals corresponds to the fracture stress. The fracture stress was 0.57 ± 0.26 MPa, which is similar to a previous report [7].

In previous studies, the plastic deformation due to the slip deformation has been observed in native protein crystals

via the microindentation method [6,20–22]. However, in this study of the macroscopic deformation, rather than plastic deformation, brittle fractures occurred in the native crystals. This difference of the deformation behavior could be considered by the relationship between the specimen and the crack size, as reported in brittle materials such as ceramics [23].

The stress-strain behavior of the one-week-cross-linked crystals showed interesting phenomena. Rather than brittle fractures, plastic deformation occurred in these crystals. This plastic deformation exhibited yield-point phenomena with upper and lower yield points. In other words, when the maximum stress was achieved, the stress decreased with increasing strain and reached a minimum value, as shown in Fig. 1(b). Beyond the lower yield point, the stress gradually increased with increasing strain. The deformation observed may be classified as stage I deformation, which manifests as an easy-glide region of dislocations in typical face-centered-cubic crystals such as Cu crystals [24]. Stage I deformation was observed in most of the cross-linked protein crystals at strains of up to approximately 60% during compression.

Macroscopic observation of the crystal surfaces revealed many slip lines. A bundle of inhomogeneous slip lines appeared as slip bands, as shown in Fig. 1(f). Moreover, slip traces along the $[112]$ and $[11\bar{2}]$ directions were observed on the crystal surface, and the width of the bundle was approximately $100 \mu\text{m}$, shown as line A in Fig. 1(f). The angle between the trace of line A and the $[001]$ direction

was approximately 57° . The angle between the $[112]$ and $[001]$ directions was 55° , which agreed with the measured angle. This means that the double slips with $[112]$ and $[11\bar{2}]$ occur. The appearance of the slip lines indicates that plastic deformation is controlled by a dislocation mechanism. However, work hardening was not observed in the stress-strain curves. The two types of dislocations in the $[112]$ and $[11\bar{2}]$ directions do not appear to interact with each other; therefore, sessile dislocations could not nucleate owing to dislocation reactions.

According to the dislocation model, the yield-point phenomena of crystalline materials can be explained by the nucleation, multiplication, and motion of dislocations. Two types of yield-point phenomena have been reported. One is due to the strong dislocation-locking effect of impurity atoms or the so-called Cottrell effect, which leads to the pronounced stress drop required for deformation after yielding in some alloys [25] and is typically seen in low-carbon Fe crystals. The other is due to the dynamic behaviors of dislocation multiplication and motion in accordance with the Johnston-Gilman yielding theory [26]. Three conditions are important in this theory. First, the initial mobile-dislocation density must be low. Second, the dislocation velocity corresponding to the applied stress must be low. Finally, the dislocations should multiply rapidly. These behaviors have been observed in single crystals with free and/or low dislocation density, such as in semiconducting crystals composed of Ge and Si [27–30]. In a previous report, the grown-in dislocation density of native T-HEWL crystals was estimated to be $\sim 10^2 \text{ cm}^{-2}$ [31], which means high perfection. As the grown-in dislocation density of cross-linked protein crystals is expected to be low, they are also expected to have higher perfection. In the case of the cross-linked T-HEWL crystals, the stress drops in the stress-strain curve could be mainly explained by the Johnson-Gilman theory. The fracture stress of the cross-linked crystals is considered to be higher than their yield stress because of cross-linking, although fracture primarily occurs in the native crystals because of their relatively lower fracture stress. The characteristics of the plastic deformation associated with induced dislocations are discussed later. The results thus far indicate that brittle materials are transformed into ductile materials via cross-linking.

We investigated the relationship between the cross-linking time and mechanical properties, such as the Young's modulus and lower yield stress, of the crystals. Figure 2 shows the dependence of the Young's modulus and lower yield stress of the crystals on the cross-linking time. The 1-day-cross-linked protein crystals showed brittle fractures and did not exhibit a plastic deformation. As seen in Fig. 2(a), the Young's modulus greatly increased and reached the maximum value after 1 day of cross-linking. The Young's modulus of the 1–7-day-cross-linked crystals was $389 \pm 36 \text{ MPa}$, which is approximately 5.8 times higher than that of native crystals. However, lower yield points appeared for samples with cross-linking time for 2 days. It gradually increased with increasing cross-linking time for samples cross-linked over 3 days, as shown in Fig. 2(b). The average lower yield stress of the 3–7-day-cross-linked crystals was $12.5 \pm 0.8 \text{ MPa}$. Both the Young's modulus and lower yield stress depended on the cross-linking time, although the times required to reach stable

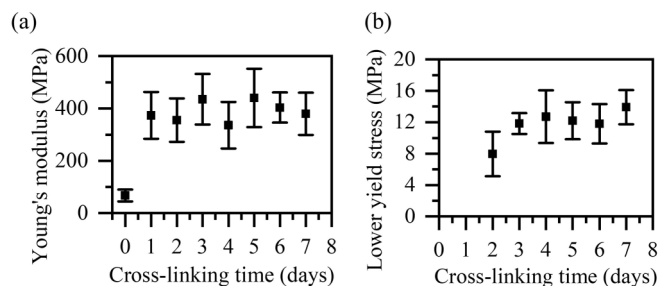


FIG. 2. Relationship between the cross-linking time and (a) Young's modulus and (b) lower yield stress of the cross-linked crystals. The error bars in (a) and (b) indicate the standard deviation (plots, average value).

values differed. The cross-linking reaction is predominantly controlled by the interactions of Lys13 and Arg45. Buch *et al.* revealed through x-ray structural analysis that the cross-linking reaction at Arg45 occurs faster than that at Lys13 [32]. The inter-(111)-plane bonding, which is slip plane, is only Lys13-Lys13. Therefore, the yield stress required to cut the bond and induce slip deformation is a delayed increase. Details regarding the slip planes will be discussed later. In addition, the discrepancy in the time dependence of these parameters may be attributed to the fundamental mechanisms of both phenomena. Also, it is considered that this time dependence is due to the difference of the amount of the cross-linking. In the short reaction period such as 1 day, the inside of the crystal is brittle, similar to the native crystal, and the crack nucleation and propagation easily occur. Young's modulus is insensitive to the number of cross-linked molecules because of the deformation of the entire sample, so it increases quickly after 1 day of cross-linking. After the inside of the crystal is cross-linked fully by the longer time, the lower yield stress reaches maximum values. The dislocation motion could be more sensitive for a number of cross-linked molecules because the core structure of dislocations depends on the intermolecular potential [33].

Results and discussion: Identification of slip systems activated by cross-linking. We consider the slip systems of the 1-week-cross-linked crystals. Figure 3(a) shows a schematic diagram of the as-grown form of a T-HEWL crystal. Figures 3(b), 3(c), and 3(d) show x-ray topographic images of the 110, $\bar{1}10$, and 200 diffractions, respectively. The corresponding schematics of the crystals are shown in each figure. Figure 3(c) corresponds to Fig. 3(b) rotated by 90° around the $[001]$ direction, and Fig. 3(d) corresponds to Fig. 3(b) rotated by -45° around the $[001]$ direction. Here, we focus on the two contrasts in these topographs. A clear contrast in crystal shape can be observed for each diffraction, indicating that the compressed crystal maintains its single crystallinity. Another contrast in the lines denoted A and B is observed in the 110 reflection, as shown in Fig. 3(b). The contrast in these lines is in good agreement with the slip traces observed in the optical images shown in Fig. 1(f). However, the line contrast seen in Fig. 3(b) disappeared, as shown in Fig. 3(c). Moreover, planar shapes with a white contrast, denoted as planes A and B, appeared in the 200 reflection, as shown in Fig. 3(d).

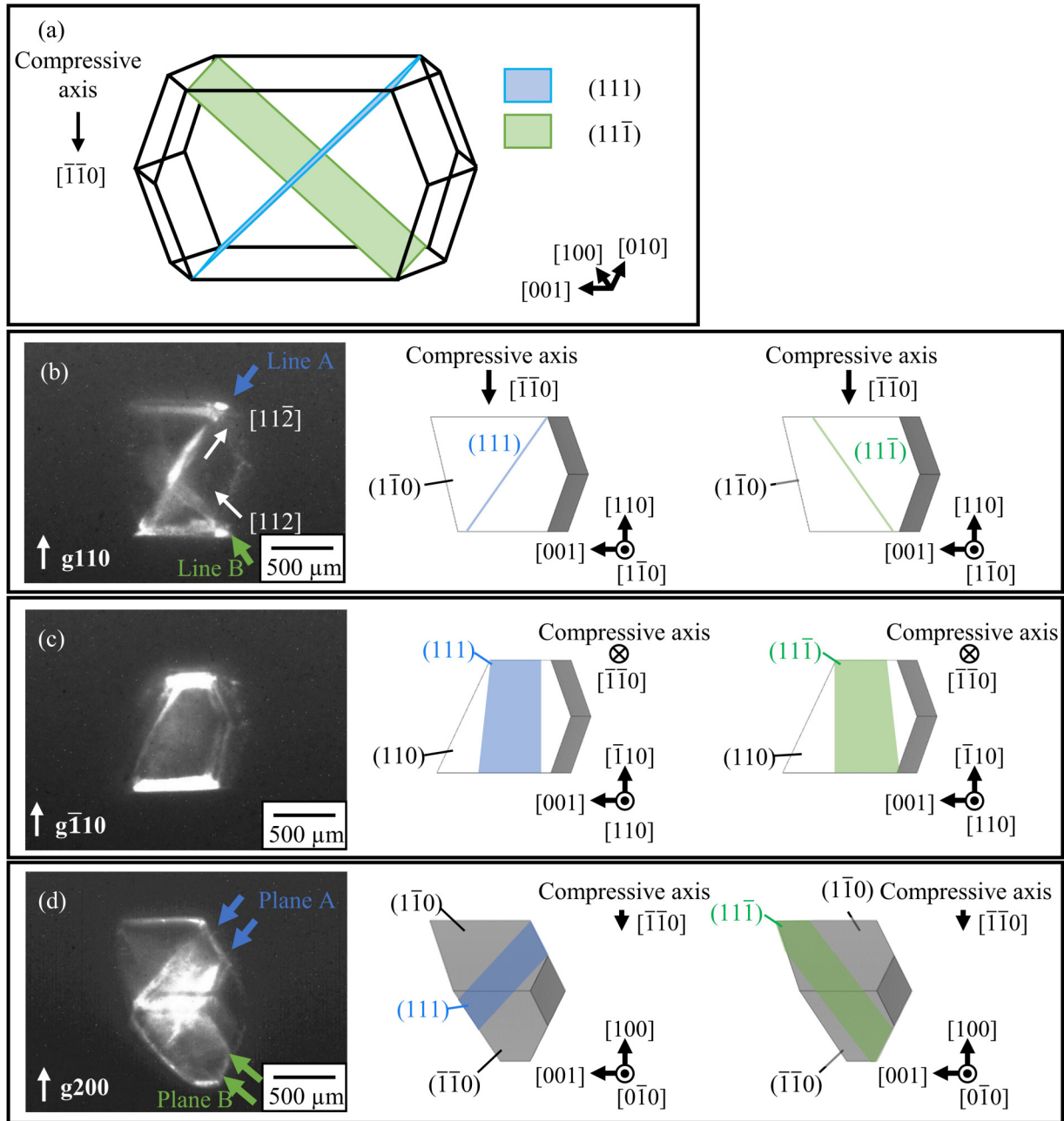


FIG. 3. (a) Schematic diagram of a T-HEWL crystal with the ideal form. [(b)–(d)] Typical x-ray topographs (median filtered images) and corresponding schematics of the crystal orientation taken from the (b) 110, (c) $\bar{1}10$, and (d) 200 reflections after the compression test. Based on the compression test, this sample had approximately 3.5% plastic strain. The schematic figures of crystal morphology were prepared using VESTA software [39].

Next, we consider the slip systems introduced during the compression tests. The Burgers vectors of the induced dislocations were identified using synchrotron x-ray topography. The Burgers vectors of dislocations can be determined based on the invisibility criterion for dislocation images ($\mathbf{g} \cdot \mathbf{b} = 0$, where \mathbf{g} and \mathbf{b} are the diffraction and Burgers vectors, respectively). The contrasts of lines A and B in Fig. 3(b) are invisible in the $\bar{1}10$ reflection, as shown in Fig. 3(c). According to the invisibility criterion, the possible Burgers vectors for the slip traces denoted by line A lie in $[11\bar{1}]$, $[11\bar{2}]$, and $[2\bar{2}\bar{1}]$. Thus, the Burgers vector was assigned to $[11\bar{2}]$ because $[11\bar{1}]$ and

$[2\bar{2}\bar{1}]$ are not parallel to the slip traces observed in the optical images, as shown in Figs. 1(f) and 1(g) (the angles between $[001]$ and $[11\bar{2}]$ and the slip line observed in the crystal are 54° and 57° , respectively). Subsequently, the slip planes were determined. Based on Weiss’s law of zones, the (111) , (201) , and (110) planes are possible slip planes along the Burgers vector $[11\bar{2}]$. We considered the Schmidt factor to identify the possible slip planes. For reference, the d spacing and Burgers vectors of the native and cross-linked crystals are listed in Tables II and III, respectively. The Schmidt factor is proportional to the critical resolved shear stress [34]. The Schmidt

TABLE II. Magnitude of the d spacing of the lattice plane in native and cross-linked HEWL crystals.

Lattice plane	d spacing (nm)	
	Native	Cross-linked
(100)	7.91	7.89
(001)	3.79	3.70
(101)	3.42	3.35
(110)	5.59	5.58
(111)	3.14	3.08
(201)	2.74	2.70

factors for the (111), (201), and (110) planes are estimated as 0.46, 0.40, and 0.00, respectively, as summarized in Table IV. Thus, one of the slip systems for the slip traces denoted by line A in Fig. 1(f) was assigned as (111) $[11\bar{2}]$. Similarly, the slip system for the slip traces denoted by line B in Fig. 1(f) was characterized as $(11\bar{1}) [112]$ (the Schmidt factor for this line is 0.46, similar to that of line A). In previous investigation, the slip deformation of native crystals with (110) $[1\bar{1}0]$ was detected through a microindentation test [6]. However, in this study, the slip system remains inactive due to a Schmidt factor of 0.00. Additionally, the slip system of (111) $[11\bar{2}]$ was not observed in native crystals. This suggests that cross-linking enables the activation of the slip system.

Figure 4(a) shows a schematic of the (111) $[11\bar{2}]$ slip system in a unit cell of the cross-linked crystals when compressed in the $[\bar{1}\bar{1}0]$ direction. Two slip systems move at an angle in response to compression and intersect. In general, slip planes have the highest density of atoms or molecules, that is, they are the most widely spaced, and the slip direction is always parallel to the Burgers vector of the dislocation responsible for slip deformation [34]. As shown in Tables II and III, the assigned (111) $[11\bar{2}]$ slip system in the cross-linked crystals has a large Burgers vector (11.31 nm) on planes with a narrow lattice spacing (3.07 nm). In continuous elastic bodies, the self-energy of a dislocation, E , is proportional to the shear modulus μ and the square of the Burgers vector, b^2 , that is, $E \sim \mu b^2$ [34]. Therefore, as a general criterion, the dislocation in a crystal should have the minimum Burgers vector, that is, the minimum lattice vector. However, previous studies in which the slip systems of tetragonal, orthorhombic, and triclinic HEWL crystals were characterized using Vickers

TABLE III. Magnitude of the Burgers vector in native and cross-linked HEWL crystals.

Burgers vector	b (nm)	
	Native	Cross-linked
[100]	7.91	7.89
[001]	3.79	3.68
[101]	8.77	8.71
[110]	11.19	11.16
[111]	11.79	11.75
[112]	11.34	11.31

TABLE IV. Estimated Schmidt factor of cross-linked HEWL crystals.

Slip system	Schmidt factor
(111) $[11\bar{2}]$	0.46
$(11\bar{1}) [112]$	0.46
(201) $[11\bar{2}]$	0.40
$(1\bar{1}0) [11\bar{2}]$	0.00

hardness experiments demonstrated that the slip systems in these crystals are unique because various slip systems are activated by the applied stress [19,20,21]. Almost all slip systems without the minimum dislocation energy estimated by dislocation theory have been observed in other protein crystals using x-ray topography [35], which means stress-induced dislocations without the shortest Burgers vector and with the largest d spacing are activated in the protein crystals. The characteristics of this slip system may be associated with the strong bonds formed between HEWL molecules owing to cross-linking.

Cross-linking reactions between the glutaraldehyde and HEWL molecules are not random events. Cross-linking between amino acid residues (such as lysine and arginine) and glutaraldehyde forms $-C=N-$ bonds [10]. Cross-linking with glutaraldehyde mainly involves lysine (Lys13) and arginine (Arg45) residues in HEWL molecules [32]. The reaction is initiated at the preferred cross-linking sites depending on the arrangement of the HEWL molecules. The free aldehyde groups of glutaraldehyde are highly reactive and exhibit different tendencies for self-polymerization depending on environmental factors such as pH and linker concentration in aqueous media [36].

Figure 4(b) shows schematics of the molecular arrangement and slip system of the cross-linked crystals based on their [111] (top view of the (111) direction) and $[1\bar{1}0]$ (side view of the (111) direction) views, which were drawn based on their structural information (Protein Data Bank (PDB) ID, 2hu3 [10]). The HEWL molecules are schematically drawn as ellipses, and the waviness of the crystallographic planes is ignored because protein molecules have complex shapes. As shown in Fig. 4(b), the amino acid residues Lys13 and Arg45 are diagonally arranged on the HEWL molecule. Cross-linking between HEWL molecules occurs at Lys13-Lys13 and Arg45-Arg45. In the side view of (111), interplanar bonds corresponding to the bonds \star and \star in the top view are indicated by lines. The only interplanar bonds are Lys13-Lys13 cross-linking bonds. Six intra-cross-linking bonds and two inter-cross-linking bonds are observed on the crystallographic (111) plane of the unit cell (the area is 37.3 nm²). Thus, the molecular interactions in the (111) plane of the cross-linked HEWL crystals are stronger than those of the native crystals. We considered that the cross-linked (111) plane becomes more stable against stress so that the (111) plane can act as the slip plane.

The appearance of plastic deformation in the crystals depends on the nucleation and motion of dislocations under an applied stress. In native HEWL crystals with weak intermolecular interactions, the fracture stress is much

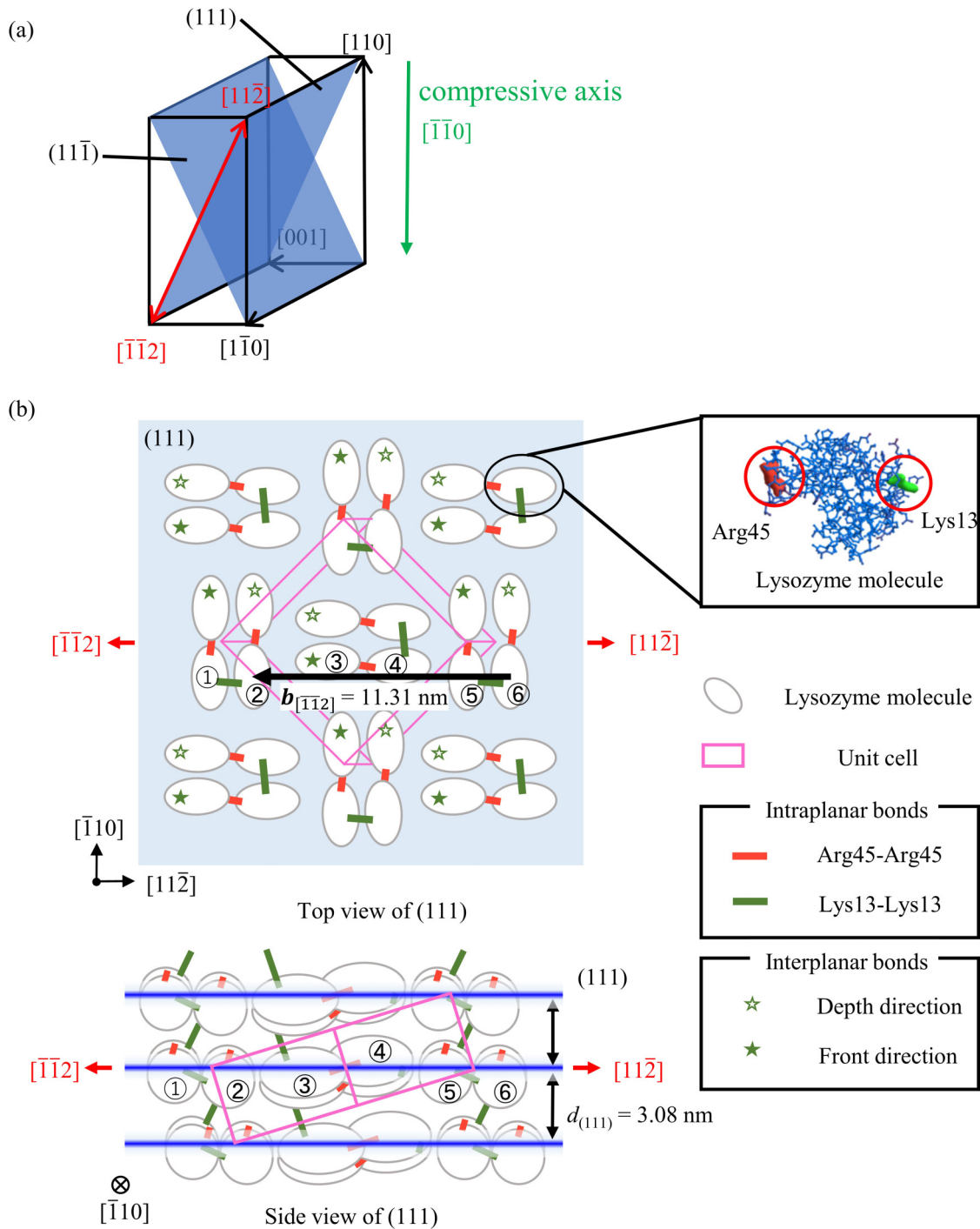


FIG. 4. Schematic illustrations of the slip systems and molecular arrangements of the cross-linked crystals. (a) Slip system (111) $[11\bar{2}]$ when compressed in the $[\bar{1}\bar{1}0]$ direction. The two blue planes represent {111}, and the red line shows the $\langle 112 \rangle$ direction on {111} planes. (b) Molecular arrangement based on the $[111]$ (top view of the (111) direction) and $[\bar{1}\bar{1}0]$ (side view of the (111) direction) planes. White ellipses indicate lysozyme molecules, and red, green, and pink parallelepipeds represent Arg-Arg bonds, Lys-Lys bonds, and a unit cell, respectively. The cross-links of Lys13-Lys13 (denoted as green lines) and Arg45-Arg45 (denoted as red lines) appear in the (111) slip plane. The bonds in the (111) slip plane are drawn as lines, while the bonds in the depth and front directions are represented by ☆ and ★, respectively. Here, ☆ is directed toward the lower region of the (111) plane, and ★ is directed toward the upper region of the (111) plane. In the side view of the (111) plane, the blue lines on the molecular packing represent the (111) slip plane with a d spacing of 3.08 nm. In (b), the numbers 1–6 assigned to the HEWL molecules in top view correspond to those of the side view.

lower than the yield stress required for the nucleation and motion of dislocations. Consequently, fracture is favored over plastic deformation. However, in the case of cross-linked protein crystals, the fracture stress is higher than the yield stress because of the strong intermolecular interactions induced by cross-linking, resulting in plastic deformation. The ductile properties of cross-linked protein crystals indicate their great potential for various material applications with enzymatic activity for biocatalysis and biosensing [37,38].

Conclusion. In summary, cross-linking is widely known to be useful for strengthening protein crystals. In this study, we quantitatively evaluated the mechanical properties of cross-linked protein crystals by compression tests. It was found that cross-linked protein crystals were plastically deformed and showed typical stress-strain curves with the upper and lower yield points. Thus, brittle native protein crystals were transformed into ductile protein crystals by cross-linking. After compression testing, slip traces were clearly observed in the cross-linked protein crystals, with the Burgers vectors of

the slip systems determined by using x-ray topography. This shows that plastic deformation during compression primarily occurs due to dislocation, multiplication, and motion, causing slip deformation within the crystal. The ductility of protein crystals exhibited by cross-linking indicates their immense potential for material applications with enzymatic activity for biocatalysis and biosensing. It is anticipated to open up new possibilities for biomaterials development.

Acknowledgments. We would like to thank Dr. K. Wako of Yokohama Soei University for his critical comments on our data analysis. Synchrotron monochromatic-beam x-ray topography was performed using the BL20B beamline at the Photon Factory of the High Energy Accelerator Research Organization (KEK) with the approval of the Program Advisory Committee (Proposals No. 2021G022 and No. 2023G030). This work was supported by PRESTO, the Japan Science and Technology Agency (JPMJPR1995), and the Japan Society for the Promotion of Science (JSPS) KAKENHI Grants-in-Aid for Scientific Research (Grants No. 19K23579, No. 21K04654, and No. 23H01305).

-
- [1] M. A. Meyers and K. K. Chawla, *Mechanical Behavior of Materials*, 2nd ed. (Cambridge University Press, Cambridge, 2008).
- [2] A. McPerson, *Crystallization of Biological Macromolecules* (Cold Spring Harbor Laboratory, New York, 1999).
- [3] B. W. Matthews, *J. Mol. Biol.* **33**, 491 (1968).
- [4] T. Pan, B. Maity, S. Abe, T. Morita, and T. Ueno, *Nano Lett.* **23**, 6744 (2023).
- [5] A. A. Chernov, *J. Struct. Biol.* **142**, 3 (2003).
- [6] T. Kishi, R. Suzuki, C. Shigemoto, H. Murata, K. Kojima, and M. Tachibana, *Crystals* **7**, 339 (2017).
- [7] R. Suzuki, A. Karasawa, A. Gomita, M. Abe, K. Kojima, and M. Tachibana, *ACS Appl. Bio Mater.* **6**, 965 (2023).
- [8] M. Kubiak, K. Storm, I. Kampen, and C. Schilde, *Cryst. Growth Des.* **19**, 4453 (2019).
- [9] E. Yan, H. Cao, C. Zhang, Q. Lu, Y. Ye, J. He, L. Huang, and D. Yin, *RSC Adv.* **5**, 26163 (2015).
- [10] Y. Wine, N. Cohen-Hadar, A. Freeman, and F. Frolow, *Biotechnol. Bioeng.* **98**, 711 (2007).
- [11] V. N. Morozov and T. Y. Morozova, *Biopolymers* **20**, 451 (1981).
- [12] M. Tachibana, K. Kojima, R. Ikuyama, Y. Kobayashi, and M. Ataka, *Chem. Phys. Lett.* **332**, 259 (2000).
- [13] H. Koizumi, M. Tachibana, and K. Kojima, *Phys. Rev. E*, **73**, 041910 (2006).
- [14] S. Speziale, F. Jiang, C. L. Caylor, S. Kriminski, C.-S. Zha, R. E. Thorne, and T. S. Duffy, *Biophys. J.* **85**, 3202 (2003).
- [15] M. Kubiak, J. Solarczek, I. Kampen, A. Schallmey, A. Kwade, and C. Schilde, *Cryst. Growth Des.* **18**, 5885 (2018).
- [16] M. Tachibana and K. Kojima, *Curr. Top. Cryst. Growth Res.* **6**, 35 (2002).
- [17] R. Diamond, *J. Mol. Biol.* **82**, 371 (1974).
- [18] C. A. Schneider, W. S. Rasband, and K. W. Eliceiri, *Nat. Methods* **9**, 671 (2012).
- [19] R. Suzuki, M. Abe, K. Kojima, and M. Tachibana, *J. Appl. Cryst.* **54**, 163 (2021).
- [20] M. Tachibana, Y. Kobayashi, T. Shimazu, M. Ataka, and K. Kojima, *J. Cryst. Growth*, **198/199**, 661 (1999).
- [21] R. Suzuki, T. Kishi, S. Tsukashima, M. Tachibana, K. Wako, and K. Kojima, *Philos. Mag.* **96**, 2930 (2016).
- [22] R. Suzuki, C. Shigemoto, M. Abe, K. Kojima, and M. Tachibana, *CrystEngComm* **23**, 3753 (2021).
- [23] H. Masuda, K. Morita, M. Watanabe, T. Hara, H. Yoshida, and T. Ohmura, *Acta Mater.* **203**, 116471 (2021).
- [24] J. Fridel, *Dislocations* (Pergamon Press, New York, 1964).
- [25] A. H. Cottrell, and B. A. Bilby, *London Edinburgh Dublin Philos. Mag. J. Sci.* **42**, 573 (1951).
- [26] W. G. Johnston and J. J. Gilman, *J. Appl. Phys.* **30**, 129 (1959).
- [27] K. Sumino, S. Koda, and K. Kojima, *Mater. Sci. Eng.* **13**, 263 (1974).
- [28] H. Alexander, *Dislocations in Covalent Crystals*, Dislocation in Solids Vol. 7 (North-Holland, Amsterdam, 1986).
- [29] A. George, *Mater. Sci. Eng. C* **233**, 88 (1997).
- [30] I. Yonenaga, *Eng. Fract. Mech.* **147**, 468 (2015).
- [31] H. Koizumi, M. Tachibana, I. Yoshizaki, and K. Kojima, *Philos. Mag.* **85**, 3709 (2005).
- [32] M. Buch, Y. Wine, Y. Dror, S. Rosenheck, M. Lebediker, R. Giordano, R. M. F. Leal, A. N. Popov, A. Freeman, and F. Frolow, *Biotechnol. Bioeng.* **111**, 1296 (2014).
- [33] S. Tamaki, N. Ide, I. Okada, and K. Kojima, *Jpn. J. Appl. Phys.* **37**, 6115 (1998).
- [34] J. P. Hirth and J. Lothe, *Theory of Dislocations*, 2nd ed. (Wiley, New York, 1982).
- [35] R. Suzuki, M. Tachibana, H. Koizumi, and K. Kojima, *Acta Mater.* **156**, 479 (2018).
- [36] I. Migneault, C. Dartiguenave, M. J. Bertrand, and K. C. Waldron, *BioTechniques* **37**, 790 (2004).
- [37] S. Lopez, L. Rondot, C. Leprêtre, C. Marchi-Delapierre, S. Ménage, and C. Cavazza, *J. Am. Chem. Soc.* **139**, 17994 (2017).
- [38] M. Conejero-Muriel, I. Rodríguez-Ruiz, C. Verdugo-Escamilla, A. Llobera, and J. A. Gavira, *Anal. Chem.* **88**, 11919 (2016).
- [39] K. Momma and F. Izumi, *J. Appl. Cryst.* **44**, 1272 (2011).